RSC Advances

ROYAL SOCIETY OF CHEMISTRY

www.rsc.org/advances

ARTICLE TYPE www.rsc.org/xxxxxx | XXXXXXXX

Chitin based hybrid composites reinforced with graphene derivatives: a nanoscale study

Joaquín Antonio González,[a] María Emilia Villanueva,[a] María Luz Peralta Ramos,[a] Claudio Javier Pérez,[b] Lidia Leonor Piehl [c] and Guillermo Javier Copello*[a]

Received (in XXX, XXX) Xth XXXXXXXXX 200X, Accepted Xth XXXXXXXXX 200X
First published on the web Xth XXXXXXXXX 200X
DOI: 10.1039/b00000000x

In this work, we present two novel nanostructured hybrid materials based on a chitin matrix loaded with increasing amounts of graphene oxide and reduced graphene oxide nanosheets (nGO and rGO respectively). Both kind materials (Chi:nGO and Chi:rGO) were studied using different spectroscopic and rheological techniques with the aim of understanding the interaction mechanism between chitin and nGO/rGO and explaining how the type of filler and its proportion affects its reinforcement. The production of these hybrids represents not only the obtention of low-cost materials with mechanical resistance but also a good opportunity for developing materials with several applications according to their composition. The nGO and rGO were characterised through FT-IR and ESR for the determination of oxidation degree of each nanofiller. Then, the hybrids were spectroscopically analysed with FT-IR, ESR and SAXS which demonstrated that the components do not interact through covalent bondings and the nanosheets are well-dispersed among the chitin matrix. Finally, a rheological behavior assay results was performed and its results were analysed in terms of G' and η^*. In short, all the results allowed us to conclude that nGO acts as a more efficient reinforcer than rGO due to the higher amount of hydrogen bondings established with chitin.

1. Introduction

After cellulose, chitin is the second most abundant biopolymer present mainly in the exoskeletons of insects and the shells of crustaceans, including shrimp and crab, as well as other invertebrates, such as marine sponges.[1,2] It is a polysaccharide with a structure consisting predominantly of unbranched chains of β-(1→4)-2-acetoamido-2-deoxy-D-glucose. Although chitin is a semicrystalline biopolymer with nano-sized fibrillar morphology and excellent material properties, most chitin is discarded from fishing and food industries. Therefore, it is a low-cost biopolymer and it would be important to promote the use of chitin as an eco-friendly material. This interest comes from its biocompatibility, biodegradability, low toxicity and capacity to form mechanically stable materials that can be used for protein sorption, water remediation, food wrapping, tissue engineering, wound dressing and drug delivery systems.[3–6]

In the most of the cases, the development of polysaccharide based hydrogels usually include a cross-linker with the aim of improving the mechanical resistance of the final material. Examples of these cross-linkers are epichlorohydrin, glutaraldehyde, methacrylate, isocyanates, among others. [7,8] In those materials, the reinforcement is directly related with the degree of covalent interactions between the matrix and the cross-linker. Nevertheless, the use of cross-linkers is usually associated with the loss of reactive sites, changes in the adsorption selectivity, toxicity of the cross-linker, etc. [8] In order to avoid some of these disadvantages the reinforcement can be pursued using fillers instead of cross-linkers. The insertion of nanofiller between the chains of a polymer matrix represents the reinforcement of the polymer at the molecular scale in the same way than the fibers at the macroscopic scale even at low filler percentages. In the last two decades the use and types of nanofillers (such as nanoclays, talc, silica and carbon allotropes) has been rising and increasing the offer of new nanocomposites.[9] The introduction of fillers within polymeric networks have been based on the seeking of a desire property. Usually, the success of these developments is supported by empirical results and is rarely deduced from the interaction of the polymeric matrix and the filler component. Understanding the mechanism of this interaction would mean a key step towards tailored synthesis of materials with desirable chemical and mechanical properties.

The recent technological advances in the nanotechnology field have driven the use of nanostructures as fillers. In this regard, graphene derivatives have gained increased interest.[10] Graphene is a one-atom-thick planar sheet with sp^2 bonded carbon atoms that are densely packed in a honeycomb crystal lattice. Unlike graphene, graphene oxide (GO) has in its structure a large number of functional groups such as hydroxyls, epoxides, carbonyls and carboxyls that increase it solubility in hydrophilic solvents and reactivity. Several researchers have reported the use of graphene oxide nanosheets (nGO) as fillers for polysaccharide based materials, such as starch, alginate, cellulose and chitosan, mainly aiming for the reinforcement of their mechanical properties.[11–13] Regarding to the reduced graphene oxide (rGO), it can be obtained through different kinds of reduction of nGO like photothermal, elecrochemical and chemical reduction in liquid phase, being the last one the most feasible and cheap to implement at large scale. After the chemical reduction, there is a recovery of the sp^2 features and the amount of oxidized groups disappear, but not completely.

Owing to their geometry and nanostructure, nGO and rGO can be considered similar nanofillers; however, their different chemical composition based on the degree of oxidation and

sp^2 regions would provide the opportunity to synthesize novel nanocomposites with different applications according to the type of filler used. This concept encourages the studying of how both graphene derivatives behave and interact with the same polysaccharide matrix.

In this work we present two types of gel-like hybrid materials based on a chitin network reinforced with increasing amounts of graphene oxide and reduced graphene oxide nanosheets (nGO and rGO, respectively) acting as nanofillers in both cases. The nanostructure of the composites was characterized using different spectroscopic techniques and the degree of reinforcement was approached by a rheological analysis. The main aim of the research is the elucidation of the principal mechanism of interaction between the chitin chains with the nGO and rGO.

2. Experimental

2.1. Materials

Natural graphite powder (< 125 mm particle size) was purchase from Bitter (UK). Chitin from crab shells (DA: 92%; Mr ≈ 400,000) was obtained from Fluka (USA). Calcium chloride dihydrate was purchased from Anedra (Argentina); L-ascorbic acid and methanol were obtained from Ciccarelli (Argentina) and Sintorgan (Argentina) respectively. Water was filtered and deionized with a MilliQ, Millipore system (Milford, MA, USA). All other reagents were of analytical grade.

2.2. Preparation of graphene oxide (nGO) and reduced graphene oxide nanosheets (rGO)

Graphite oxide were prepared through Hummers method.[14] The graphite oxide was exfoliated into GO monolayer nanosheets (nGO) by sonication at 35 kHz for 30 min after dispersion in citrate buffer (0.4 M; pH: 4.20). Then, the suspension was centrifuged and the pellet was washed with water and then with methanol. The methanol was removed by heating in a stove at 60 ºC and the nGO was then stored at room temperature.

The reduced graphene oxide (rGO) was obtained through chemical reduction of nGO using Lascorbic acid as reduction reagent.[15] The nGO powder (100 mg) and L-ascorbic acid (5.0 g) were diluted in 100 mL of ultrapure water. The mixture was kept at 90 ºC under stirring in water bath for 2 h. Then, the solution was centrifuged at 2000 rpm for 10 min, re-suspended in water and washed several times by re-suspension/centrifugation cycles. Finally, the supernatant was discarded and the pellet dried at 80 ºC. In order to determine qualitatively the degree of oxidation of the nGO and the reduction yield of rGO they were analysed by FT-IR, Raman spectroscopy and Electron Spin Resonance (ESR).

2.3. Preparation of chitin hydrogel and Chi:nGO and Chi:rGO hybrid materials

The chitin suspension was obtained following the method proposed by Tamura et al.[16] Briefly, in order to prepare a transparent calcium solvent, 42.5 g of calcium chloride dihydrate was suspended in 50 mL of methanol and refluxed for 30 min at 82 ºC to a state of near-dissolution. Chitin powder (1 g) was suspended in the calcium solvent and refluxed for 2 h at 90 ºC with stirring. Different mass ratios of chitin and nGO were mixed by thorough agitation in order to obtain four types of hybrid materials with different chitin to graphene oxide ratios (Chi:nGO): (20:1), (3:1), (1:1), and (0.4:1). The same procedure and proportions were used to obtain the Chi:rGO hybrids. The mixtures were poured between two glasses spaced by glass slides of known width and then submerged in methanol until they gelled. Finally, the gels were subjected to several water incubations in order to wash out all of the methanol and $CaCl_2$ residues. Blank chitin gels without nGO or rGO were obtained by a similar procedure and named Chi gels. The gels were cut in a certain geometry depending on the experiments.

2.4 Spectroscopic and microscopic characterisation

The nGO, rGO, chitin and dry hybrids powders were placed in a quartz tube and ESR spectra were recorded at 20 ºC in an X-band ESR Spectrometer Bruker EMX plus (Bruker Instruments, Inc., Berlin, Germany). The spectrometer settings were: sweep width 150.0 G; centre field 3515 G; microwave power 0.1 to 250 mW and conversion time 5.12 ms. For g factor calculation, Diphenylpicrylhydrazyl (DPPH, Aldrich) (g = 2.0036) was used as an internal standard. Fourier Transform Infrared (FT-IR) transmission spectra were acquired in the range 4000 – 400 cm^{-1} using a FT-IR Spectrometer (Nicolet 360). All samples were previously dried for 24 h at 60 ºC to avoid water related band interference. Raman spectra of graphite, nGO and rGO powders were recorded with excitation laser beam of 413 nm (3 mW laser power) in backscattering geometry using a confocal microscope coupled to a single stage spectrograph (Jobin Yvon XY 800) equipped with a CCD detector. The investigation of the ultrastructure of the nanocomposites was performed by Small Angle X-ray Scattering using the SAXS2 beamline of the National Synchrotron Light Laboratory (LNLS), Campinas, Brazil. The SAXS measurements were performed at room temperature in transmission geometry with λ=1.55 Å (8 keV). The 2D SAXS spectra were monitored using a photomultiplier and detected on a marCCD 165 detector. A sample to-detector distance of 0.5 and 2 m and an exposure time of 60 s were used. The samples were placed with their surfaces perpendicular to the direction of the incident X-ray beam and parallel to the X-ray detector. The scattering intensity (I) was measured as a function of the scattering vector (q) from 0.07 to 5.3 nm^{-1}. The background and parasitic scattering were determined by using an empty sample holder and were subtracted for each measurement. X-rays powder diffraction (XRD) transmission patterns were recorded in the diffraction angular range of $5° \leq 2\theta \leq 60°$ using a PANalytical X'Pert Pro diffractometer working in the reflection geometry and equipped with a graphite monochromator on the diffracted beam (Cu-Ka radiation).The nanosheets size and exfoliation was observed using a transmission electron microscope (TEM, Zeiss 109).

2.5 Rheological behaviour

Amplitude sweeps were performed first in order to determine the linear viscoelastic range (LVR). The elastic or storage modulus, G' (ω), the viscous or loss modulus, G'' (ω) and complex viscosity (η^*) of the studied materials were obtained in small-amplitude oscillatory shear flow experiments using a rotational rheometer from Anton Paar (MCR-301) provided with a CTD 600 thermo chamber. The tests were performed using parallel plates of 25 mm diameter and a frequency range of 0.1–500 s^{-1}. The measurements were carried out at room temperature (20 ºC). All the tests were performed using small strains (γ = 3.0%) to ensure the linearity of the dynamic responses.[17] All the runs were repeated using different samples. The gap width used was 700 - 800 µm.

3. Results and discussion

3.1 Spectroscopic characterisation of nGO and rGO

FT-IR, Raman spectroscopy and ESR were used to asses the nGO and rGO synthesis. The FTIR spectra of graphite, nGO and rGO are shown in ESI 1. The nGO spectrum shows an increase in the bands corresponding to oxidized groups, which confirms the chemical exfoliation of graphite. In the spectrum of nGO, the slight band at 1220 cm^{-1} is attributed to the C–O–C bond stretching which demonstrates the formation of epoxy groups.[15] The presence of carboxyl and carbonyl functional groups can also be detected at 1400 and 1725 cm^{-1}, which correspond to C–OH and C=O stretching, respectively. After reduction, the peaks at 1400 and 1725 cm^{-1} are attenuated suggesting a decrease of carbonyl and carboxyl groups. The peak at 1600 cm^{-1}, which corresponds to the absorption of carbonyl groups plus C=C in the nGO, suffers a narrowing and a slight right shift in the rGO. This would account for a reduction of the carbonyl moieties and an increase of the C=C functional groups. Furthermore, it can be seen an increment in the relative intensity of the epoxy band at 1220 cm^{-1} accompanied by a fall of the peak absorption at 1040 cm^{-1} (C-OH stretching). Therefore, the reduction by L-ascorbic acid diminishes the amount oxidized groups from carbonyl and carboxyl moieties and regenerates unsaturated sp^2 carbon structures. The Raman spectrum of pristine graphite (Fig. 1) presents a sharp G peak at 1575 cm^{-1} corresponding to the first-order scattering of the E2g mode, a 2750 cm^{-1} 2D peak and a small D peak at 1375 cm^{-1} (A1g mode).[18,19] In the nGO and rGO spectra it could be seen the broadening of G peak, an increase of D peak and the disappearance of 2D peak. Since G peak accounts of primary in-plane vibration and 2D is related to the stacking of the sheets, these changes would imply the exfoliation and disordering of graphite into nanosheets.[20] Among nGO and rGO spectra it can also be seen a slight increase in I_D/I_G ratio that would indicate the size reduction of the in-plane sp^2 domains together with further unorganization probably related to the reduction process, as has been previously reported.[18,21,22] This is in accordance to the ESR results. Fig. 2 shows graphite, nGO and rGO ESR spectra. The most evident change is the variation of the linewidth signal (ΔHpp) of the graphene derivatives. The unorganization of graphitic domains together with the introduction of defects in the nanosheets is evidenced by the transformation of the broad Dysonian line of graphite (ΔHpp = 11.1 G) (due to skin effect) into a Lorentzian curve in nGO, due to the appearance of an intense sharp free radical-like derivative

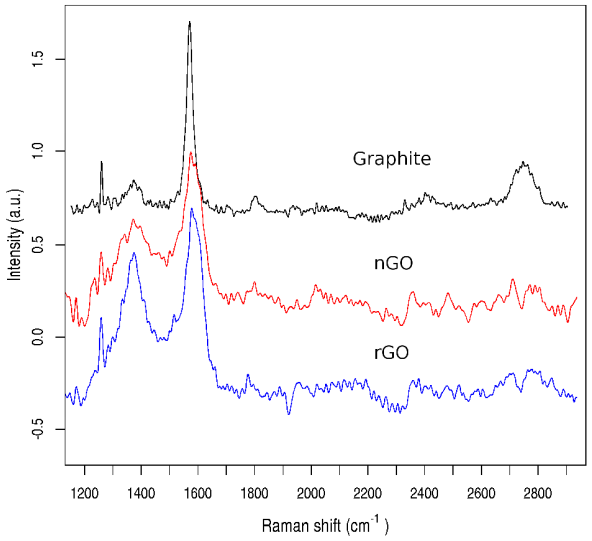

Fig. 1 Raman spectra of graphite, nGO and rGO.

peak (ΔHpp = 1.9 G).[23,24] According to Collins et al., this sharp signal became from unpaired mobile π electrons stabilized by resonance energy in large condensed ring structures, many of which probably contain oxygen.[25] After reduction, the oxidized groups are expected to decrease leading to a drop in the intensity of the signal, as it is observed in rGO spectra. Also, the broadening seen in the rGO signal (ΔHpp = 2.5 G), due to a shortening of spin-lattice relaxation time, has been attributed to the presence of graphitic-like structures.[24,25] Recent studies have proven that the average signal is a superposition of the signals from free conduction electrons, localized edge states and molecular-type paramagnetic states.[26] The same g factor was obtained from the three samples and its value was 2.0037 which is in accordance with previous studies.[27] The XRD results (ESI 2) show a characteristic spectrum of graphite with a high intensity peak at 2θ = 26.5º, which corresponds to an interplanar distance equal to 0.34 nm, due to the stacking of the graphene sheets that interact through Van der Waals forces.[28] The amorphous nature and the presence of oxidized groups in nGO converged in a XRD spectrum with no appreciable peaks. Moreover, these oxidized moieties contribute to the disorganization of the sheets and increase the distance among them.[29] In the case of rGO it can be seen a peak shift to lower values of 2θ (24.6°), which accounts for greater interplanar distance of the nanosheet probably due to presence of remaining oxidized groups from nGO. Also, the broadening of the rGO signal would indicate a high degree of exfoliation. Using the Scherrer's equation the estimated number of stacked layers was found to be minor of 10 sheets. This would indicate that during reduction the restacking of the rGO sheets would not be enough organized to achieve a graphitic like stacking.[26] This was also observed in the TEM images of the nanosheets (ESI 3) where nGO and rGO appears similar in size but rGO shows few sheets of restacking.

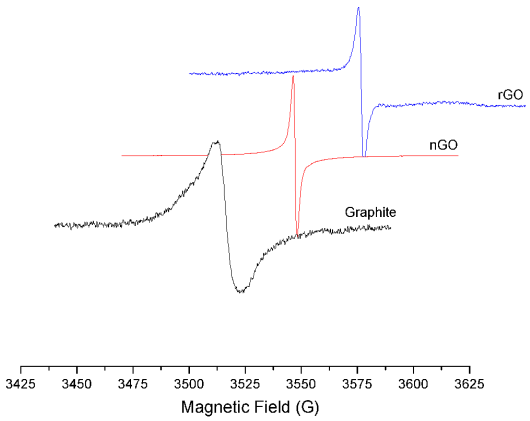

Fig 2. ESR spectra of graphite, nGO and rGO.

3.2 Characterisation of the hybrids

3.2.1 FT-IR spectroscopy

Comparing the hybrids FT-IR spectra, one can see the increase and decrease of the relative intensities of the characteristic bands of each component according to their proportion in the material (Fig. 3). For example, as nGO or rGO increases the intensity of its characteristic bands also increases. In all the cases the typical bands corresponding to chitin can be observed, especially in those materials with high chitin proportion.[30] In the spectra of the hybrids it could not be observed any new bands or the disappearance of any bands present in the individual spectra of Chi, nGO or rGO. This indicates that the interaction between chitin and both kinds of nanosheets probably does not involve the formation of a new functional group detectable by the FTIR experimental conditions.

3.2.2 SAXS analysis

The SAXS technique was used to obtain structural information of the gels network in the nanometric scale. Fig. 4 shows the SAXS profiles of Chi gels, Chi:nGO and Chi:rGO hybrids with subtraction of nGO and rGO spectra according to the case. Aside from both 0.4:1 hybrids, all profiles follow a power-law behaviour in the q range of □0.009–0.05 Å^{-1}, above which a short knee-like middle regime with lower slope appears. This profiles are found in disordered materials with at least two structural levels. In the low q region, all spectra, fitted according to the relation $I(q) \sim q^{-\alpha}$, show values of the exponent α near to 2.5. This behaviour is indicative of scattering from fractal objects. The exponent α has also been previously related to the network density.[31–33] In contrast, chitin powder profile shows an extended power-law regime with α near to 3.5, indicative of surface fractals (Inset Fig. 4a). The dissolution and subsequent gelling of the swollen chitin would be responsible for the difference of α between chitin powder and Chi gel and hybrid materials profiles.

On the other hand, the fact that Chi gel and all hybrids scattering profiles show a similar α demonstrates that Chi gel network fractal structure is not being affected by the presence of nGO or rGO in the hybrid materials. Nevertheless, the short knee-like

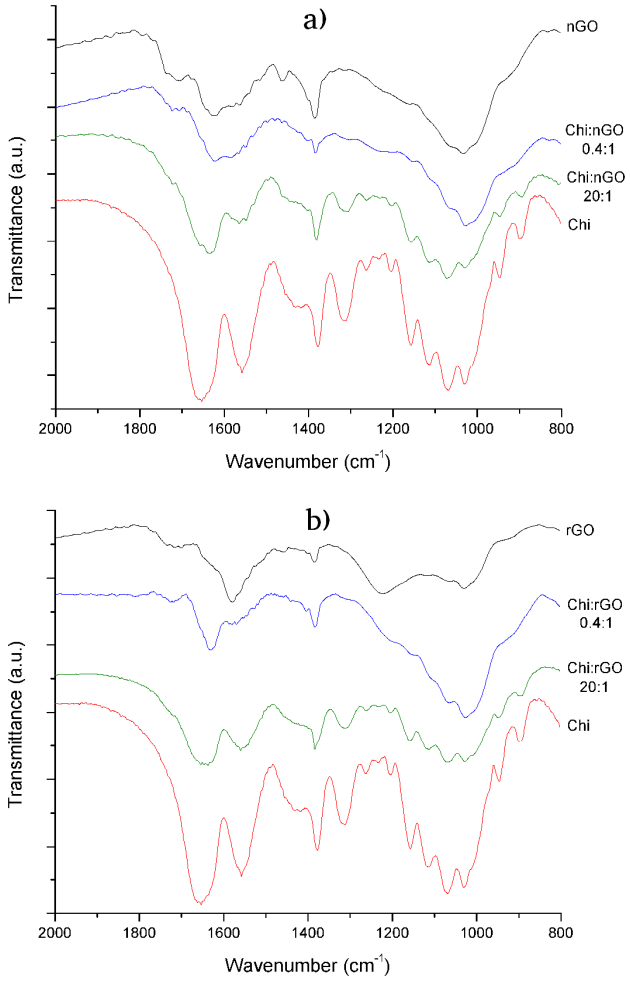

Fig 3. FT-IR spectra of Chi:nGO (a) and Chi:rGO (b) hybrids.

regime becomes less evident with the increase of nanosheet content in the hybrids, being undetectable in both 0.4:1 hybrids. This suggests that this structure level is in a lower proportion in the hybrids than in Chi gels, probably due to a hindrance effect of the nanosheets upon chitin structural organization in the gelling stage.

With the aim of describing mass fractal morphologies, Beaucage proposed a unified equation that gives insight throughout multiple structural levels of disordered materials:[32,34]

$$I(q) \approx G^{\left(\frac{-q^2 R_g^2}{3}\right)} + B^{\left(\frac{-q^2 R_{sub}^2}{3}\right)}\left(\frac{1}{q^*}\right)^P + G_s^{\left(\frac{-q^2 R_s^2}{3}\right)} + B_s\left(\frac{1}{q_s^*}\right)^{P_s}$$

where G and Gs are the Guinier prefactors for the larger and smaller structures respectively, R_g is the radius of gyration, B and B_s are prefactors specific to the Power-law scattering, which are specified as the decay exponent P and P_s respectively, $q^* = q/[\mathrm{erf}(q\, k\, R_g/6^{1/2})]^3$ and $q_s^* = q/[\mathrm{erf}(q\, k_s\, R_s/6^{1/2})]^3$.

Fig. 4a and 4b table insets indicate the R_g of each material SAXS pattern within the knee-like regime zone calculated using the Beaucage unified equation. It could be observed that neither nGO or rGO addition to the Chi gels significantly affects the R_g of the

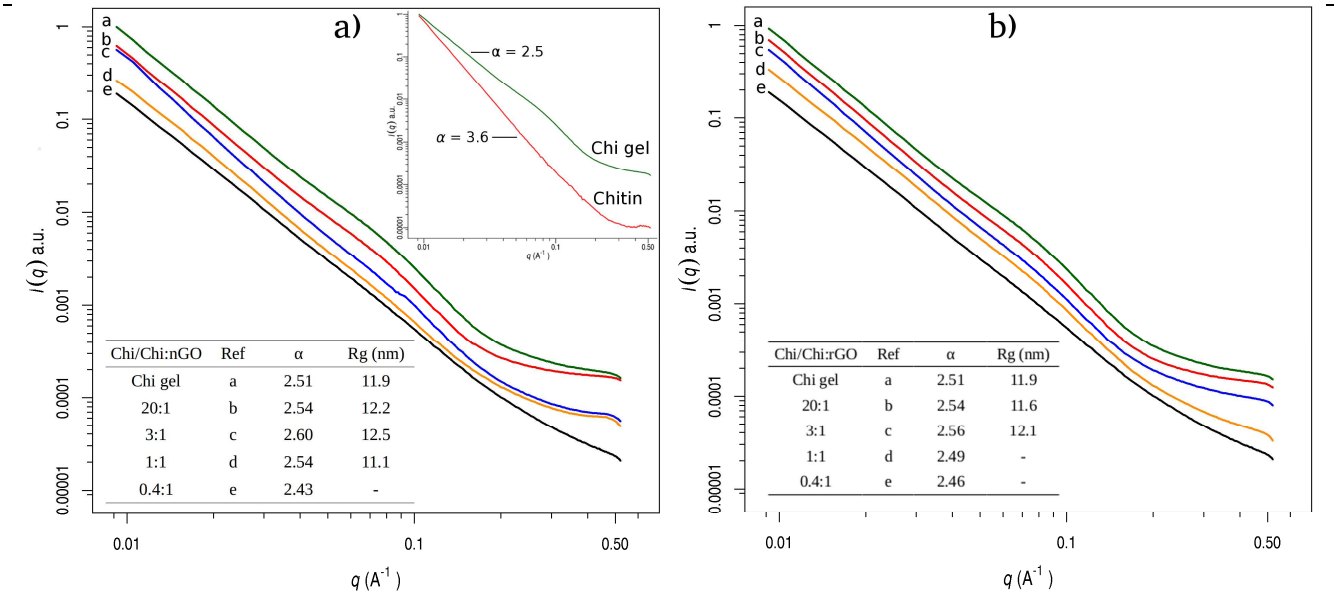

Fig 4. SAXS profiles of Chi:nGO (a) and Chi:rGO (b) hybrids. The insets in both figures show the R_g and α of each hybrid.

chitin chains. As well as in relation to the exponent α, the lack of variation of the R_g of the chitin chains, together with the decrease of the intensity of the knee-like regime would indicate that the interaction of the polysaccharide with the nanosheets do not induce new structural organizations. The lack of formation of new structural levels supports the FT-IR results were no evidence of new strong bondings could be found among hybrid components. The main changes in the hybrids structure would be therefore related to the interference of the nanosheets in the gelling of swollen chitin, thus favouring the disordered fractal structure.

3.2.3 ESR study

ESR was also used for the study of the Chi gels and Chi:nGO and Chi:rGO hybrids. ESR spectra of the hybrids show a lorentzian peak with a $g = 2.0037$. This peak would account for the nGO and rGO free radical-like signal. Chi gels did not present signal within this field (data not shown). The main difference among hybrid spectra appears in the linewidth of the free radical-like signal. The Fig. 4 shows the ESR signal linewidth of the hybrids, as a function of the percentage of nanosheets in the materials. For both type of hybrids, as the concentration of the nanosheets increase, the linewidth falls close to the values of pristine nGO and rGO. In particular, that narrowing effect is steeper in Chi:rGO hybrids, i.e. its linewidth is more sensitive to the percentage of rGO than the linewidth of Chi:nGO. This change in signal linewidths, with no detectable g value shift, is indicative of exchange narrowing from non orbital electrons.[35] Although a reduction in exchange narrowing is the main cause of line broadening, it has been pointed out that in the absence of the exchange effect, such as in the diluted compounds, the dipolar interaction broadening prevails leading to the resultant linewidth.[36] Therefore, at low nanosheet proportion, the filler particles are dispersed by the interaction with the chitin matrix providing a more pronounced dipole broadening. This behaviour would imply the interaction of chitin with the nanosheets by their oxidized groups, probably by hydrogen bonding. Moreover, in order to confirm that the broadening effect is not originated by a simple dilution of the nanosheets and the interaction is maximized during the hybrid synthesis process, the ESR signal of a chitin and nGO or rGO powder mixture (1:1) was analysed. The ΔHpp for the powder mixture was 1.9 G and 2.6 G for chitin:nGO and chitin:rGO respectively, a value close to the ones of pristine nGO and rGO respectively. This demonstrates that there is no broadening effect if the mixture is prepared by dispersion of the nanosheets in the chitin solution.

Finally, the linear decrease of ΔHpp while nGO or rGO content is increased reflects the enhancement of exchange interactions, due to the decrease in the average distance between uncoupled electronic spins. The result indicates that the material has a very good homogeneity at the nanoscale throughout all the formulation tested.[37] In this regard Tang *et al.* demonstrated that the mechanical reinforcement of a hybrid composite with rGO is proportional to the degree of dispersion of the filler among the matrix, proving the implortance of this feature.[38]

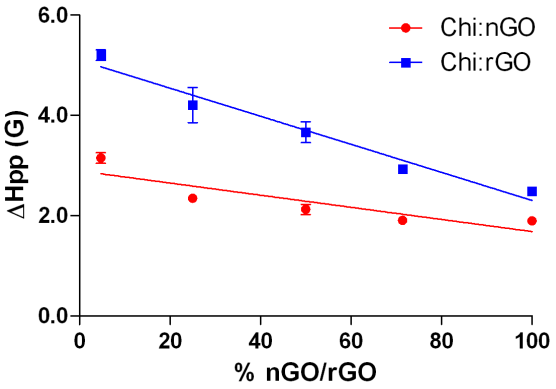

Fig 5. Variation of the ESR signal linewidth (ΔHpp) according to the percentage of nanofiller in each hybrid material.

3.2.4 Rheological behaviour

The rheological behaviour of the hybrids was analysed in order to compare the reinforcement produced by each type of nanosheet and therefore make an approach to understand the interaction

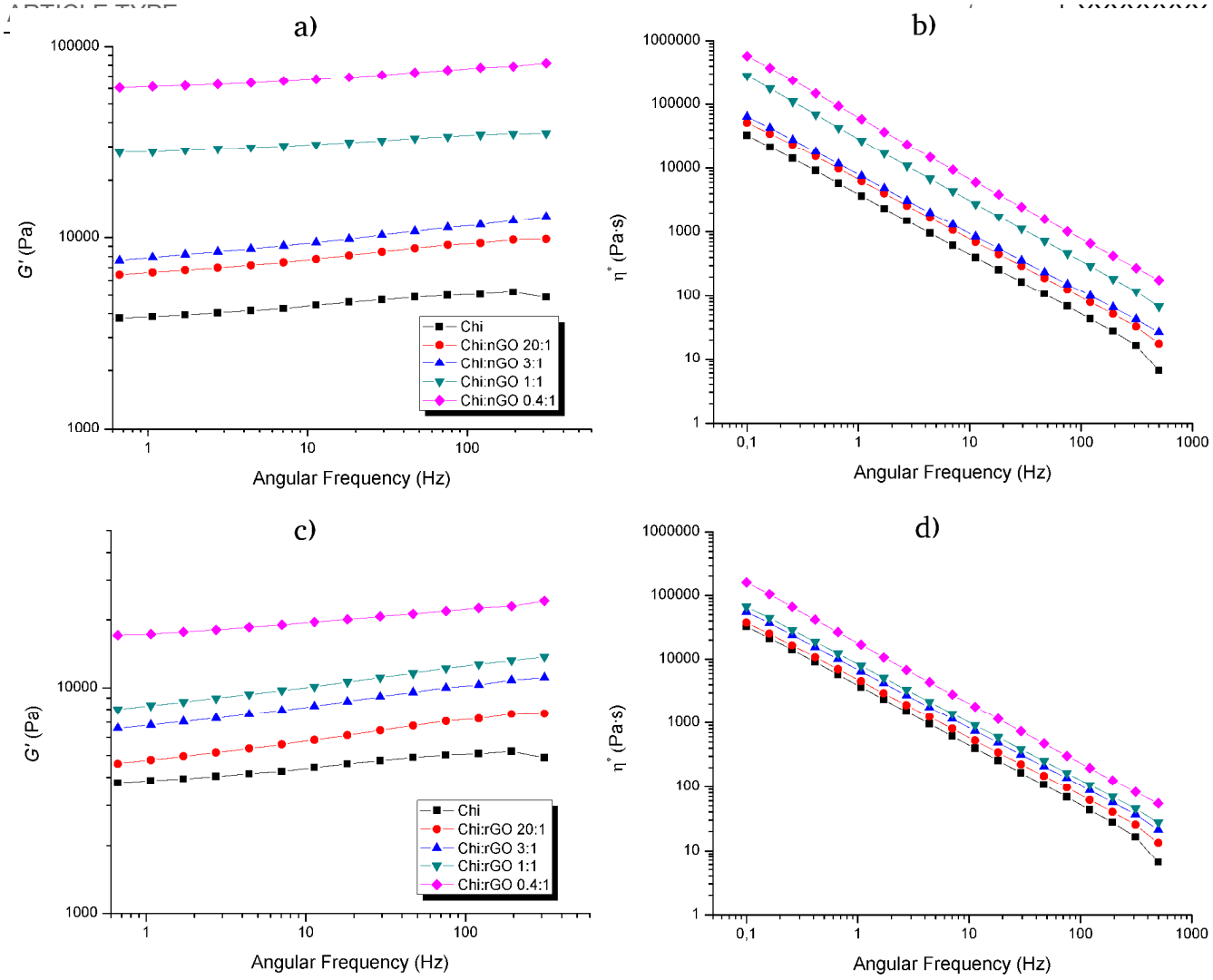

Fig 6. Storage modulus (G') and complex viscosity (η^*) frequency dependent of the Chi:nGO (a,b) and Chi:rGO (c, d) hybrids.

between the components. In the ESI 4 it can be seen that the *G'* is greater than the *G"* for all cases, which implies that the elastic component of the material is dominant over the viscous component. This is typical of a gel-like behaviour.[17] The higher values of *G'* and *G"* of both kinds hybrids, compared to Chi ones, prove that the addition of nanosheets provides mechanical reinforcement to the chitin matrix. A progressive increase of both parameters can be observed as the concentration of filler augments. Nevertheless, the *G'* and η^* values of Chi:nGO hybrids are higher than those of Chi:rGO prepared with the same amount of nanosheets, indicating that the nGO generates a stiffer material in comparison to rGO (Fig. 6). For example, at a frequency of 1 Hz and for the same Chi:nanosheet ratio (1:1), rGO duplicates the complex viscosity while nGO is seven times greater with respect to the Chi gel. This results support the previous ESR data where a greater interaction between the nGO and chitin is proposed based on the higher capability of the allotrope to establish more hydrogen bondings with the polysaccharide chains. The complex viscosity of the hybrids decreases almost linearly with the increase of the frequency, showing shear thinning behaviour which is probably due to the structure of the hybrid polymer network (Fig. 6b and 6d). Also, slopes of the viscosity curves, around -0.9, indicates that both systems behave similar to a polymer network with predominantly permanent links.[17]

Conclusions

It has been demonstrated that the introduction of both kinds of nanofillers, one with greater hydrophilicity than the other (nGO and rGO respectively), in a chitin gel matrix improved significantly the mechanical features of the material. The spectroscopic FT-IR analysis showed that the components do not interact between them by the formation of new covalent bondings nor the formation of a new functional group. The SAXS plots and its further mathematical analysis suggest that the Chi gel has two main nanostructured levels. However, in the hybrid gels, one of them decreases or partially disappears as the material is loaded with higher amounts of nanosheets. Regarding to the ESR, the linear narrowing effect of the nGO and rGO proportion, i.e. low *ΔHpp* values at higher filler ratios, indicates a good dispersion of the nanosheets among the chitin matrix. Taking into account the moieties involved in the generation of the ESR signal and the results of FT-IR, it is concluded that the hydrogen bondings are the main proposed mechanism of interaction. Furthermore, the rheological assay proved that higher amounts of nanosheets provide more reinforcement, especially in those materials with

nGO which has more available oxidized groups for the interaction with the chitin matrix through hydrogen bondings.

Acknowledgements

J.A.G. is grateful for his doctoral fellowship granted by Universidad de Buenos Aires. M.E.V. is grateful for her doctoral fellowship granted by Consejo Nacional de Investigaciones Científicas y Técnicas. The authors are grateful to the Brazilian Synchrotron Light Laboratory (LNLS) for SAXS facilities. This work was supported with grants from Universidad de Buenos Aires (UBACYT 20020130100780BA) and Consejo Nacional de Investigaciones Científicas y Técnicas (PIP 11220120100657CO).

Notes and references

[a] *Cátedra de Química Analítica Instrumental, Facultad de Farmacia y Bioquímica, Universidad de Buenos Aires (UBA), IQUIMEFA (UBA-CONICET), Junín 956, C1113AAD Buenos Aires, Argentina;* Tel/fax: +54 11 49648254; *E-mail: gcopello@ffyb.uba.ar*
[b] *Instituto en Investigaciones en Ciencia y Tecnologías de Materiales, Universidad de Mar del Plata, (CONICET), Juan B. Justo 4302, CP7600 Mar del Plata, Argentina*
[c] *Cátedra de Física, Facultad de Farmacia y Bioquímica, Universidad de Buenos Aires (UBA), Junín 956, C1113AAD CABA, Argentina*
† Electronic Supplementary Information (ESI) available. See
DOI: 10.1039/b000000x/

References

1 W. L. Teng, E. Khor, T. K. Tan, L. Y. Lim and S. C. Tan, *Carbohydr. Res.*, 2001, **332**, 305–316.
2 M. Wysokowski, V. V. Bazhenov, M. V. Tsurkan, R. Galli, A. L. Stelling, H. Stöcker, S. Kaiser, E. Niederschlag, G. Gärtner, T. Behm, M. Ilan, A. Y. Petrenko, T. Jesionowski and H. Ehrlich, *Int. J. Biol. Macromol.*, 2013, **62**, 94–100.
3 S. Ifuku and H. Saimoto, *Nanoscale*, 2012, **4**, 3308–3318.
4 R. Muzzarelli, *Carbohydr. Polym.*, 1983, **3**, 53–75.
5 S. Mangalathillam, N. S. Rejinold, A. Nair, V.-K. Lakshmanan, S. V. Nair and R. Jayakumar, *Nanoscale*, 2012, **4**, 239–250.
6 A. Bhatnagar and M. Sillanpää, *Adv. Colloid Interface Sci.*, 2009, **152**, 26–38.
7 W. E. Hennink and C. F. van Nostrum, *Adv. Drug Deliv. Rev.*, 2012, **64, Supplement**, 223–236.
8 G. Crini, *Prog. Polym. Sci.*, 2005, **30**, 38–70.
9 D. M. Marquis, C. Chivas-Joly and É. Guillaume, *Properties of nanofillers in polymer*, INTECH Open Access Publisher, 2011.
10 Y. Zhu, S. Murali, W. Cai, X. Li, J. W. Suk, J. R. Potts and R. S. Ruoff, *Adv. Mater.*, 2010, **22**, 3906–3924.
11 J. Fan, Z. Shi, M. Lian, H. Li and J. Yin, *J. Mater. Chem. A*, 2013, **1**, 7433–7443.
12 A. M. Pandele, M. Ionita, L. Crica, S. Dinescu, M. Costache and H. Iovu, *Carbohydr. Polym.*, 2014, **102**, 813–820.
13 N. D. Luong, N. Pahimanolis, U. Hippi, J. T. Korhonen, J. Ruokolainen, L.-S. Johansson, J.-D. Nam and J. Seppälä, *J. Mater. Chem.*, 2011, **21**, 13991–13998.
14 W. S. Hummers Jr and R. E. Offeman, *J. Am. Chem. Soc.*, 1958, **80**, 1339–1339.
15 J. Zhang, H. Yang, G. Shen, P. Cheng, J. Zhang and S. Guo, *Chem. Commun.*, 2010, **46**, 1112–1114.
16 H. Tamura, H. Nagahama and S. Tokura, *Cellulose*, 2006, **13**, 357–364.
17 J. D. Ferry, *Viscoelastic properties of polymers*, John Wiley & Sons, 1980.
18 F. Tuinstra and J. L. Koenig, *J. Chem. Phys.*, 1970, **53**, 1126–1130.
19 A. C. Ferrari, J. C. Meyer, V. Scardaci, C. Casiraghi, M. Lazzeri, F. Mauri, S. Piscanec, D. Jiang, K. S. Novoselov and S. Roth, *Phys. Rev. Lett.*, 2006, **97**, 187401.
20 I. Childres, L. A. Jauregui, W. Park, H. Cao and Y. P. Chen, *Dev. Photon Mater. Res.*, 2013.
21 S. Stankovich, D. A. Dikin, R. D. Piner, K. A. Kohlhaas, A. Kleinhammes, Y. Jia, Y. Wu, S. T. Nguyen and R. S. Ruoff, *Carbon*, 2007, **45**, 1558–1565.
22 J. Gao, F. Liu, Y. Liu, N. Ma, Z. Wang and X. Zhang, *Chem. Mater.*, 2010, **22**, 2213–2218.
23 F. J. Dyson, *Phys. Rev.*, 1955, **98**, 349.
24 S. S. Rao, A. Stesmans, Y. Wang and Y. Chen, *Phys. E Low-Dimens. Syst. Nanostructures*, 2012, **44**, 1036–1039.
25 R. L. Collins, M. D. Bell and G. Kraus, *J. Appl. Phys.*, 1959, **30**, 56–62.
26 F. Tampieri, S. Silvestrini, R. Ricco, M. Maggini and A. Barbon, *J. Mater. Chem. C*, 2014, **2**, 8105–8112.
27 C. V. Pham, M. Krueger, M. Eck, S. Weber and E. Erdem, *Appl. Phys. Lett.*, 2014, **104**, 132102.
28 S. Park, J. An, J. R. Potts, A. Velamakanni, S. Murali and R. S. Ruoff, *Carbon*, 2011, **49**, 3019–3023.
29 J. Oh, J.-H. Lee, J. C. Koo, H. R. Choi, Y. Lee, T. Kim, N. D. Luong and J.-D. Nam, *J. Mater. Chem.*, 2010, **20**, 9200–9204.
30 Y. Saito, J. L. Putaux, T. Okano, F. Gaill and H. Chanzy, *Macromolecules*, 1997, **30**, 3867–3873.
31 C. J. Brinker, K. D. Keefer, D. W. Schaefer, R. A. Assink, B. D. Kay and C. S. Ashley, *J. Non-Cryst. Solids*, 1984, **63**, 45–59.
32 G. Beaucage, *J. Appl. Crystallogr.*, 1996, **29**, 134–146.
33 S. Choudhary and S. R. Bhatia, *Carbohydr. Polym.*, 2012, **87**, 524–530.
34 G. Beaucage, *J. Appl. Crystallogr.*, 1995, **28**, 717–728.
35 M. G. Siswanto, N. P. Bo, H. Neubacher and L. C. Burton, *Rubber Chem. Technol.*, 1988, **61**, 269–280.
36 B. N. Misra and S. K. Gupta, *Bull. Chem. Soc. Jpn.*, 1973, **46**, 3067–3069.
37 M. Chipara, D. Hui, P. V. Notingher, M. D. Chipara, K. T. Lau, J. Sankar and D. Panaitescu, *Compos. Part B Eng.*, 2003, **34**, 637–645.
38 L.-C. Tang, Y.-J. Wan, D. Yan, Y.-B. Pei, L. Zhao, Y.-B. Li, L.-B. Wu, J.-X. Jiang and G.-Q. Lai, *Carbon*, 2013, **60**, 16–27.